Improving the Performance of P3HT–Fullerene Solar Cells with Side-Chain-Functionalized Poly(thiophene) Additives: A New Paradigm for Polymer Design

Jose M. Lobez,[†,§] Trisha L. Andrew,[‡,§] Vladimir Bulović,[‡,*] and Timothy M. Swager[†,*]

[†]Department of Chemistry and [‡]Department of Electrical Engineering and Computer Science, Massachusetts Institute of Technology, 77 Massachusetts Avenue, Cambridge, Massachusetts 02139, United States. [§]These authors contributed equally to this work.

ABSTRACT The motivation of this study is to determine if small amounts of designer additives placed at the polymer–fullerene interface in bulk heterojunction (BHJ) solar cells can influence their performance. A series of AB-alternating side-chain-functionalized poly(thiophene) analogues, P1–6, are designed to selectively localize at the interface between regioregular poly(3-hexylthiophene) (rr-P3HT) and PC_nBM (n = 61, 71). The side chains of every other repeat unit in P1–6 contain various terminal aromatic moieties. BHJ solar cells containing ternary mixtures of rr-P3HT, PC_nBM, and varying weight ratios of additives P1–6 are fabricated and studied. At low loadings, the presence of P1–6 consistently increases the short circuit current and decreases the series resistance of the corresponding devices, leading to an increase in power conversion efficiency (PCE) compared to reference P3HT/$PC_{61}BM$ cells. Higher additive loadings (>5 wt %) lead to detrimental nanoscale phase separation within the active layer blend and produce solar cells with high series resistances and low overall PCEs. Small-perturbation transient open circuit voltage decay measurements reveal that, at 0.25 wt % incorporation, additives P1–6 increase charge carrier lifetimes in P3HT/$PC_{61}BM$ solar cells. Pentafluorophenoxy-containing polymer P6 is the most effective side-chain-functionalized additive and yields a 28% increase in PCE when incorporated into a 75 nm thick rr-P3HT/$PC_{61}BM$ BHJ at a 0.25 wt % loading. Moreover, devices with 220 nm thick BHJs containing 0.25 wt % P6 display PCE values of up to 5.3% (30% PCE increase over a control device lacking P6). We propose that additives P1–6 selectively localize at the interface between rr-P3HT and PC_nBM phases and that aromatic moieties at side-chain termini introduce a dipole at the polymer–fullerene interface, which decreases the rate of bimolecular recombination and, therefore, improves charge collection across the active layer.

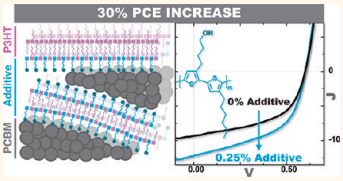

KEYWORDS: poly(thiophene) · photovoltaic · additive · interface · side-chain functionalization · recombination

Molecular and polymeric organic materials are promising replacements for the inorganic counterparts in photovoltaic cells due to their ease of processing and straightforward deposition, which allow for the fabrication of nanostructured devices on inexpensive and arbitrary substrates.[1] Most organic photovoltaic (OPV) devices require the presence of both a donor and an acceptor material to drive exciton dissociation at the interface between the two components and improve charge collection under operational bias.[2] Donor–acceptor bulk heterojunction (BHJ) solar cells formed by mixtures of regioregular poly(3-hexylthiophene) (rr-P3HT) and soluble fullerene derivatives, such as $PC_{61}BM$ and $PC_{71}BM$, are benchmark OPV structures, with average power conversion efficiencies (PCEs) of up to 5% under AM 1.5 conditions (100 mW/cm^2).[3] A variety of device and material factors limit the performance of BHJ solar cells, but the properties of the photoactive layer are the primary determinant of the maximum achievable PCE. The ideal donor–acceptor mixture in a BHJ structure should exhibit a bicontinuous network with domain widths within twice that of the exciton diffusion length and a high donor–acceptor interfacial area to favor exciton dissociation and efficient transport of separated charges to the respective electrodes.[4] In the specific case of polymer solar cells (PSCs), the miscibility between the polymer donor and the fullerene acceptor, the crystallization of the polymer and fullerene phases, and the scale of the phase separation in the BHJ thin film are all critical to the overall performance of BHJ OPVs.[5–9]

The use of additives to improve the performance of rr-P3HT/PC_nBM (n = 61, 71) solar cells by changing the morphology of the active layer has been reported in the past, but examples have been limited to the use of high boiling point alkyl dihalides that act as cosolvents[10] or main-chain block copolymers.[11–13] The use of P3HT with lower regioregularities as an additive has also been reported, and moderate increases in the open circuit voltage (V_{OC})

* Address correspondence to bulovic@mit.edu, tswager@mit.edu.

Received for review November 25, 2011 and accepted February 21, 2012.

Published online February 27, 2012
10.1021/nn204589u

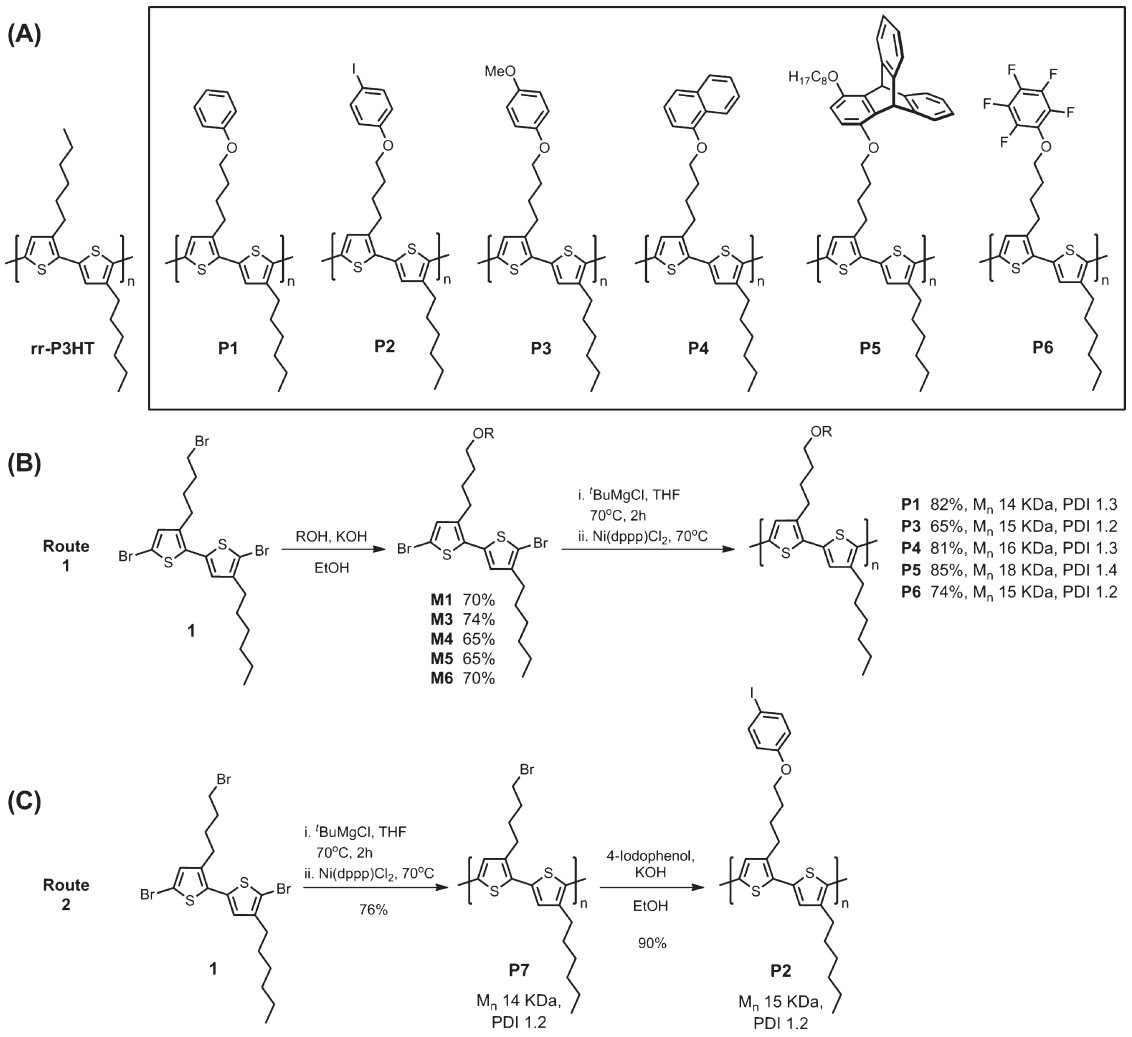

Scheme 1. (A) Structures of regioregular P3HT (rr-P3HT) and the AB-alternating, side-chain-functionalized poly(thiophene)s discussed in this study. (B) Synthesis of polymers P1−P6, excluding P2. (C) Synthesis of polymer P2. Compound 1 was synthesized following modified literature procedures (see Supporting Information for more details).

were observed, though accompanied by a decrease in the short circuit current (J_{SC}).[14] All of these approaches typically require extra processing steps or a relatively large amount of additive (at least 5 wt %) to see an improvement in the PCE.

Both the length of the side chain on the repeat unit and the regioregularity of the polymeric donor material in PSCs have been shown to have a marked effect on solar cell performance.[15−17] In some cases, an optimal nanoscale morphology was achieved with random copolymers compared to highly ordered regioregular analogues because the random copolymers could more effectively mix with the fullerene acceptor and form bicontinuous networks.[18] In comparison, fullerene molecules were found to intercalate between the side chains of an analogous highly ordered polymer and form BHJs containing nanoparticles with poor electrical connection to the top and bottom electrodes.[19,20] Different substituents have also been directly attached to a poly(thiophene) backbone with the aim of changing its band gap,[21] but this approach has proven to be less effective than using the original P3HT/$PC_{61}BM$ system. Further chemical modification of the side chains of P3HT and its resulting effect on solar cell performance is mostly unexplored, with reported examples of side-chain functionalization mainly centered on the exploration of solubility[22,23] and sensing applications.[24]

In this study, we present a new class of designer additives based on regioregular poly(thiophene)s, where the side chains of the polymer have been functionalized at the termini in every other thiophene unit. We hypothesize that mixtures of these regioregular additives with rr-P3HT/PC_nBM would demonstrate better PCEs compared to binary rr-P3HT/PC_nBM mixtures due to improved interactions at the interface between the polymer and fullerene phases enabled by side-chain functionalization. We note that our goal is not to produce champion devices but, rather, to study the effects of subtle chemical-structure modifications on a benchmark OPV material system.

TABLE 1. Photophysical Properties of P1–6

	λ_{abs} (nm)	λ_{em} ($CHCl_3$, nm)	Φ_F[b]	τ ($CHCl_3$, ns)	K_{sv} (M^{-1})/10^3[c]
rr-P3HT	452 ($CHCl_3$) 545 (film)[a]	573	0.20	0.58	2.4
P1	450 ($CHCl_3$) 550 (film)[a]	570	0.22	0.64	4.1
P2	447 ($CHCl_3$) 545 (film)[a]	571	0.12	0.57	3.3
P3	455 ($CHCl_3$) 552 (film)[a]	573	0.22	0.62	2.4
P4	440 ($CHCl_3$) 548 (film)[a]	570	0.22	0.61	3.6
P5	445 ($CHCl_3$) 540 (film)[a]	570	0.18	0.57	3.0
P6	442 ($CHCl_3$) 545 (film)[a]	575	0.20	0.60	2.8

[a] Films 40 ± 5 nm thick spun-cast from 1,2-dichlorobenzene. [b] Fluorescence quantum yields are determined against perylene in EtOH (Φ 0.94). The measurement error is 0.03. [c] Steady-state quenching constant for each polymer with $PC_{61}BM$ in $CHCl_3$.

RESULTS

Additive Design and Synthesis. As shown in Scheme 1A, six different AB-alternating side-chain-functionalized poly(thiophene) additives to the P3HT/PC_nBM system are synthesized in this study. Poly(thiophene) **P1** contains a nonconjugated phenyl moiety in its side chain in order to elucidate the effects of introducing structural complexity at side-chain termini in a benchmark polymeric donor material. To further elaborate on this concept, polymers **P2**–**6** are also explored as additives: the effects of steric bulk or congestion can be revealed by **P2**, **P4**, and **P5**, while the effects of having weak, isolated dipoles at side-chain termini can be investigated using **P3** (which contains electron-rich anisole moieties) and **P6** (which contains electron-deficient perfluorophenyl moieties). Triptycene-containing polymer **P5** is also chosen because triptycene has been reported to be capable of interacting with fullerene analogues and forming highly ordered arrays in the solid state.[25]

As shown in Scheme 1B,C, polymers **P1**–**6** are synthesized starting from bithiophene derivative **1**, which is obtained from 3-bromothiophene following modified literature procedures (see Supporting Information for detailed synthetic protocols and characterization). Monomers **M1** and **M3**–**6** are accessed in good yield by subjecting compound **1** to Williamson ether synthesis conditions with the corresponding phenol. Subsequent nickel-catalyzed Grignard metathesis (GRIM) polymerization[26–28] of **M1** and **M3**–**6** yields **P1** and **P3**–**6** in high yields (Scheme 1B).[29–31] Considering that an iodophenyl moiety could be competitively metalated under standard GRIM polymerization conditions and introduce unwanted side reactions, polymer **P2** is synthesized following route 2 (Scheme 1C). Bromobutane-containing polymer **P7** is synthesized by GRIM polymerization of **1**, and subsequent postpolymerization functionalization with 4-iodophenol yields **P2** in moderate yield and with a high degree of substitution (99%) on the side chain.

The poly(thiophene) additives thus obtained have number-averaged molecular weights (M_n) of 16 ± 2 kDa and polydispersities (PDI) of 1.3 ± 0.1. In comparison, the commercial rr-P3HT used as the majority donor material in BHJ OPVs has a M_n of 45 kDa and a PDI of 1.7.

Additive Characterization. The absorption and emission spectra of **P1**–**6** and their corresponding peak maxima in dilute chloroform solutions are both similar to those of rr-P3HT (Table 1), thus indicating that side-chain functionalization does not alter the effective conjugation length of the poly(thiophene)s. Additionally, the solution quantum yields and excited-state lifetimes of **P1**–**6** are also identical to those of commercial rr-P3HT (within the error of each measurement). Spun-cast, annealed thin films of **P1**–**6** (40 nm) displayed red-shifted absorption maxima and weak luminescence at room temperature, similar to rr-P3HT. However, unlike films of rr-P3HT, a characteristic "order peak" at 600 nm is not observed to evolve in the absorption spectra of neat thin films of **P1**–**6**. This optical order peak is assigned to interplane interactions in highly ordered crystalline regions of rr-P3HT;[32] therefore, the lack of an order peak in films of **P1**–**6** indicates that side-chain functionalization of poly(thiophene)s hinders crystallization of polymer chains.

Steady-state fluorescence quenching studies of **P1**–**6** with $PC_{61}BM$ in chloroform solutions reveal larger Stern–Volmer quenching constants (K_{sv}) for the additives compared to rr-P3HT: for example, K_{sv} values of 4.1×10^3 and 3.6×10^3 M^{-1} are measured in $CHCl_3$ for **P1** and **P4**, respectively, compared to 2.4×10^3 M^{-1} for rr-P3HT. Lifetime Stern–Volmer measurements reveal that the excited-state lifetimes of the polymers do not change significantly with increasing fullerene concentration (see Supporting Information), indicating the dominance of a static quenching mechanism. In this case, a higher value of K_{sv} can be correlated with a larger binding affinity between the fluorophore and quencher, thus indicating that the side-chain-functionalized poly(thiophene) additives have a higher binding affinity for $PC_{61}BM$ than rr-P3HT. We note that a slight increase in the excited-state lifetime of **P5** was observed in the presence of $PC_{61}BM$, which we ascribe to conformational changes in the polymer backbone induced by a triptycene–fullerene binding interaction.

X-ray diffractograms of spun-cast and annealed films of **P1**–**6** do not contain sharp diffraction signals and indicate that these neat polymer films are amorphous (see Supporting Information). This observation is consistent with the aforementioned absence of an order peak in the absorption spectra of thin films of **P1**–**6**. However, diffractograms of rr-P3HT/$PC_{61}BM$ thin films containing up to 10 wt % of **P1**–**6** reveal that the presence of up to 10 wt % of the additives does

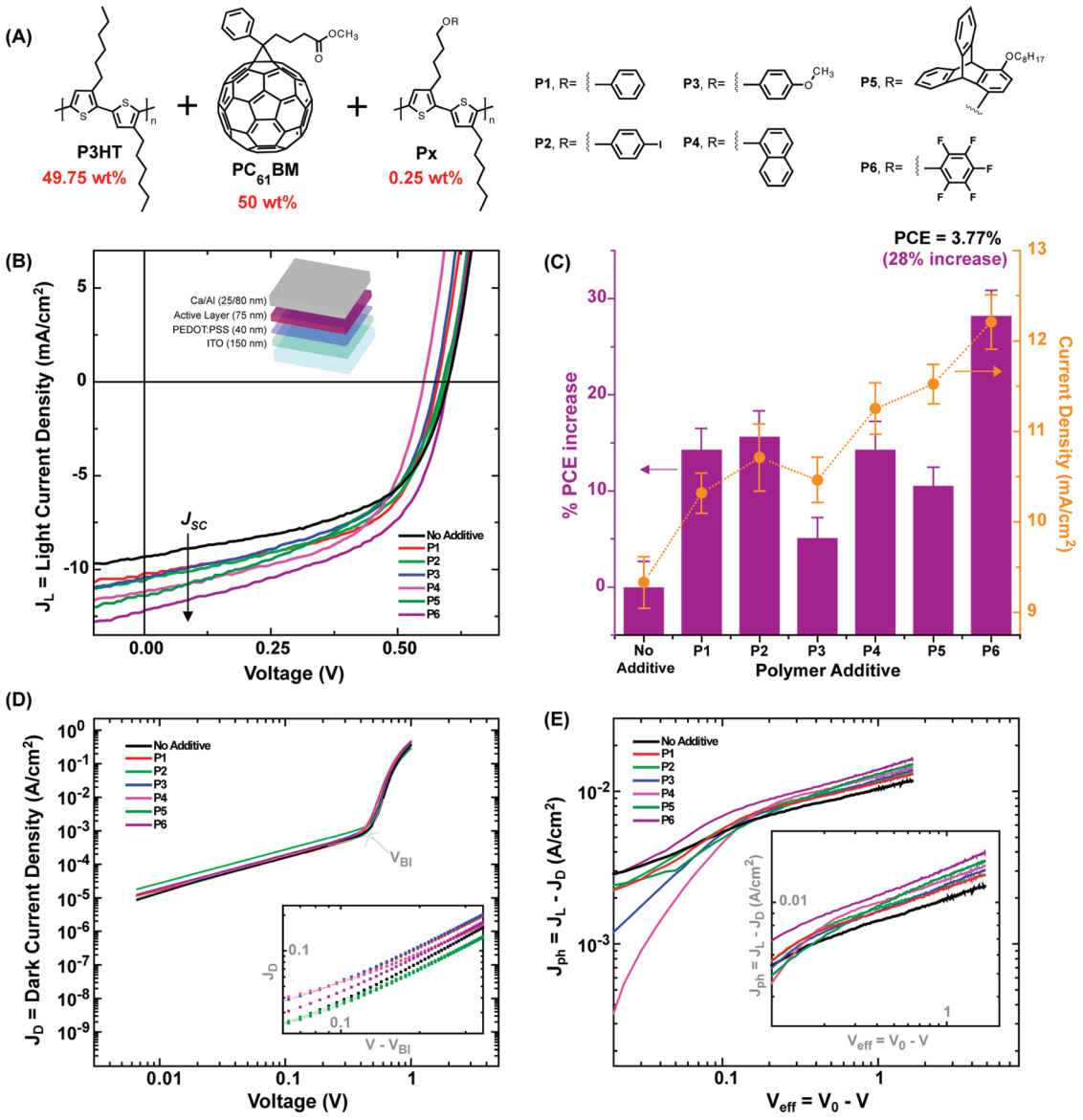

Figure 1. Performance of devices containing ternary mixtures of P3HT, P1−6, and fullerene. (A) Composition of active layer, 1:1 ratio of total polymer (P3HT + 0.25 wt % P1−6) to $PC_{61}BM$. (B) *J*−*V* curves under 1 sun for solar cells containing the active layer shown in (A). The average *J*−*V* curves over eight different devices are shown. The inset depicts the device architecture. (C) PCE increase (purple bars, left *y*-axis, % *versus* a solar cell with no additive) upon incorporation of 0.25 wt % P1−6. The variation of J_{SC} with different additives is superposed (orange, right *y*-axis). (D) Log−log plot of dark *J*−*V* curves for solar cells containing the active layer shown in (A). The inset is a plot of the dark current density, J_D, *versus* corrected voltage values. The built-in voltage, V_{BI}, is subtracted from the applied bias, *V*, to provide the corrected voltage. V_{BI} is taken as a compensation voltage $V_0 \approx V_{OC} + 0.05$ V (see ref 20). (E) Experimental photocurrent as a function of effective applied voltage, $V_{eff} = V_0 - V$, for solar cells containing the active layer shown in (A). V_0 represents the compensation voltage for which the photocurrent $J_{ph} = J_L - J_D = 0$. The inset is zoomed-in on the region where $V_{eff} > 0.1$, and the photocurrent displays a square root dependence on voltage.

not hinder lamella formation within the rr-P3HT phase of the bulk film (see Supporting Information). Thus, we infer that the lower molecular weight additives predominantly localize in amorphous regions within the rr-P3HT/$PC_{61}BM$ BHJ.

BHJ Photovoltaic Devices. The motivation of this study is to determine if small amounts of designer polymers placed at the BHJ interface can influence the performance of an OPV device. In order to investigate the effect of side-chain functionalization on solar cell performance, we fabricate solar cells containing **P1**−**6** in the active layer. Considering the disordered solid-state packing structure demonstrated by neat films of **P1**−**6**, we expected that these polymers would not perform well as *majority* donor materials in a solar cell; indeed, solar cells containing binary mixtures of **P1**−**6** and $PC_{61}BM$ displayed poor power conversion efficiencies and diode rectification. Therefore, to test the performance of **P1**−**6** as designer *additives*, we investigate OPVs containing ternary mixtures of rr-P3HT,

TABLE 2. Summary of Device Metrics for Solar Cells Containing Ternary Mixtures of P3HT, 0.25 wt % P1−6, and $PC_{61}BM$ (1 Sun Illumination)

	J_{SC} (mA/cm^2)	V_{OC} (V)	FF	R_s (Ω cm^2)[a]	R_{sh} (Ω cm^2)[b]
P3HT/$PC_{61}BM$	9.32	0.59	0.52	13.5	1280
+ 0.25 wt % **P1**	10.3	0.58	0.57	7.3	1460
+ 0.25 wt % **P2**	10.7	0.60	0.53	12.1	909
+ 0.25 wt % **P3**	10.4	0.57	0.52	7.7	1055
+ 0.25 wt % **P4**	11.2	0.55	0.54	5.8	1081
+ 0.25 wt % **P5**	11.5	0.59	0.48	12.8	1397
+ 0.25 wt % **P6**	12.2	0.60	0.53	10.7	1043

[a] Series resistance, defined as dV/dJ of the dark J−V curve at V = 0.6 V.. [b] Shunt resistance, defined as dV/dJ of the dark J−V curve at V = −0.1 − 0 V.

P1−**6**, and a fullerene. Figure 1B shows the current density−voltage (J−V) curves under illumination (averaged over eight devices) for solar cells fabricated with 1:1 P3HT/$PC_{61}BM$ and 0.25 wt % **P1**−**6**, and Table 2 provides a summary of pertinent device metrics. The J−V curve for an average P3HT/$PC_{61}BM$ solar cell without an additive is provided in black; in our hands, these reference devices (with an active layer thickness of 75 ± 5 nm) display open circuit voltage (V_{OC}) values of 0.59 ± 0.01 V, short circuit current (J_{SC}) values of 9.3 ± 0.2 mA/cm^2, and fill factors (FF) of 0.52 ± 0.03. As can be seen in Figure 1B and Table 2, the addition of small amounts of **P1**−**6** to the P3HT/$PC_{61}BM$ BHJ leads to an increase in the J_{SC} of the solar cells, while the V_{OC} and FF remain approximately the same. Notably, adding a poly(thiophene) with phenyl moieties at side-chain termini (**P1**) to the P3HT/$PC_{61}BM$ BHJ increases the observed J_{SC} by 11 ± 3%. The comparatively bulky *p*-iodophenyl analogue **P2** and the electron-rich analogue **P3** perform similarly to **P1**. Naphthyl moieties (**P4**) lead to higher observed J_{SC} than phenyl moieties (**P1**) but significantly decrease the V_{OC} of the devices. If fullerene-binding triptycene moieties (**P5**) are introduced instead of simple phenyl groups (**P1**), the J_{SC} increases by 23 ± 4%; however, **P5** decreases the FF of the resulting device. Pentafluorophenol-containing additive **P6** leads to the highest increase in overall PCE (28 ± 4%) by increasing the J_{SC} by 25 ± 3% while leaving the V_{OC} unchanged.

The series resistance (R_s) of the devices, defined as the slope of the dark J−V curves at 0.6 V, is also lower in cells containing **P1**−**6** compared to the reference P3HT/$PC_{61}BM$ device. This can be seen more clearly in the log−log representation of the dark J−V curves (Figure 1D, inset), where higher dark injection currents are observed for devices containing **P1**−**6** compared to P3HT/$PC_{61}BM$. It is also evident from semilog plots of the dark J−V curves that the side-chain-functionalized additives yield higher rectifying values compared to reference cells.

The increase in the J_{SC} upon adding 0.25 wt % side-chain-functionalized poly(thiophene)s is also manifested as an increase in the external quantum efficiency (EQE) of the devices containing **P1**−**6** (see Supporting Information). The increase in EQE cannot simply be attributed to an increase in light absorption because the absorption spectra and optical densities of 75 nm thick films of P3HT/$PC_{61}BM$ with or without 0.25 wt % **P1**−**6** are nearly identical (see Supporting Information). Therefore, this effect possibly originates from a decrease in the amount of charge recombination at the polymer−fullerene heterointerface.

Figure 1E shows the experimental photocurrent J_{ph} as a function of effective applied voltage ($V_{eff} = V_0 - V$) for solar cells containing 0.25 wt % of **P1**−**6**. The photocurrent ($J_{ph} = J_L - J_D$) is the measured current under illumination (J_L) corrected for the dark current (J_D), whereas the compensation voltage V_0 is defined as the voltage at which the photocurrent J_{ph} is 0. At voltages close to the compensation voltage ($V_0 - V <$ 0.1 V), the photocurrent is observed to increase linearly with voltage. For $V_0 - V >$ 0.1 V, the photocurrent enters a regime where a square root dependence on the effective voltage is observed. Similar behavior has been characterized in multiple conjugated polymer−fullerene BHJ OPVs, where the decrease in photocurrent for $V_0 - V >$ 0.1 V is attributed to recombination effects.[33,34] Specifically, the low mobilities or short lifetimes of free carriers (due to either recombination or trapping) are believed to limit the observed photocurrent in polymer solar cells. As seen in Figure 1E, polymer additives **P1**−**6** consistently yield higher photocurrents in the square root regime ($V_0 - V >$ 0.1 V) compared to P3HT/$PC_{61}BM$ reference cells, thus suggesting that these side-chain-functionalized additives decrease charge recombination.

To directly probe charge recombination in solar cells containing **P1**−**6** in the active layer, we performed small-perturbation transient open circuit voltage decay measurements.[35,36] In this measurement, a device is illuminated with 100 mW/cm^2 white light (1 sun) to create open circuit conditions while, simultaneously, a low-intensity pulsed 635 nm laser is used to induce a small perturbation to the V_{OC} by transiently generating additional electrons and holes. The resulting additional transient photovoltage, ΔV, will then decay with a lifetime that is determined by the recombination rate constant of the electrons and holes. Figure 2 shows representative photovoltage transients for cells with or without **P1**−**6**. The transients were taken at V_{OC} for each device with 1 sun bias light. The signals have been normalized to the same height at time zero. The actual voltage peak of all transients was <3 mV. With the exception of **P4**, additive incorporation caused a slower decay in transient photovoltage, which indicates an increase in charge carrier lifetime. As seen in the J−V curve in Figure 1, the presence of 0.25 wt % **P4** leads to a significant decrease in the V_{OC} of the resulting solar cell, and therefore, the minimal,

off-trend decrease in transient V_{OC} lifetime observed in the presence of **P4** is expected. Blends containing additive **P3**, with electron-rich *p*-anisyl moieties at side-chain termini, display multiexponential decay, thus suggesting the presence of multiple charge trapping or recombination mechanisms in this device.

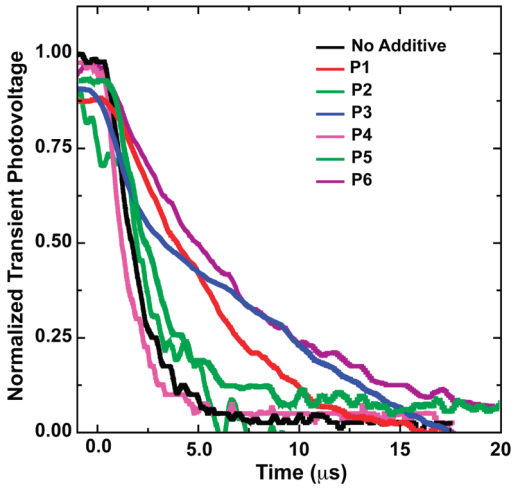

Figure 2. Normalized transient photovoltage curves at V_{OC} for solar cells containing a 1:1 ratio of total polymer (P3HT + 0.25 wt % P1−6) to $PC_{61}BM$. The *J*−*V* curves under 1 sun for these devices are shown in Figure 1. Bias illumination was 100 mW/cm^2 white light giving V_{OC} values of 0.59 V for no additive (P3HT/$PC_{61}BM$), 0.58 V for additive P1, 0.60 V for additive P2, 0.57 V for additive P3, 0.55 V for additive P4, 0.59 V for additive P5, and 0.60 V for additive P6. The secondary pulse was from a 635 nm laser, length 5 s.

Blends containing **P6** that have the highest J_{SC} values also demonstrate the slowest decay in transient photovoltage. This result can be interpreted as a decrease in the recombination rate across the polymer−fullerene heterointerface in the presence of **P6**.

Figure 3 shows the *J*−*V* curves of devices containing varying amounts of **P1**−**6** in the active layer. Appropriate metrics for the various devices examined in Figure 3 are tabulated in the Supporting Information (Table S2). In general, when additives **P1**−**6** are present in 0.25 wt %, higher PCEs are observed compared to a P3HT/$PC_{61}BM$ control. However, if greater than *ca.* 5 wt % of **P1**−**6** is used, a decrease in the PCE is observed for all additives due to increased series resistances, which manifests as a decrease in both J_{SC} and FF values. Similar observations of reduced performance have been noted for other macromolecular additives[10−15] and are attributed to a decrease in the carrier mobilities caused by phase segregation and significant disruptions of the BHJ morphology. Indeed, for higher doping concentrations, an expected increase in the series resistance can be observed, consistent with reduced carrier mobilities.

The nanoscale morphologies of the polymer−$PC_{61}BM$ films are studied using tapping-mode atomic force microscopy (AFM).[37] Surface topography (left) and phase images (right) are taken for films containing 0, 0.25, and 2.5 wt % **P6** and are shown in Figure 4. Average surface roughness values measured from the topography images of three different 5 μm × 5 μm

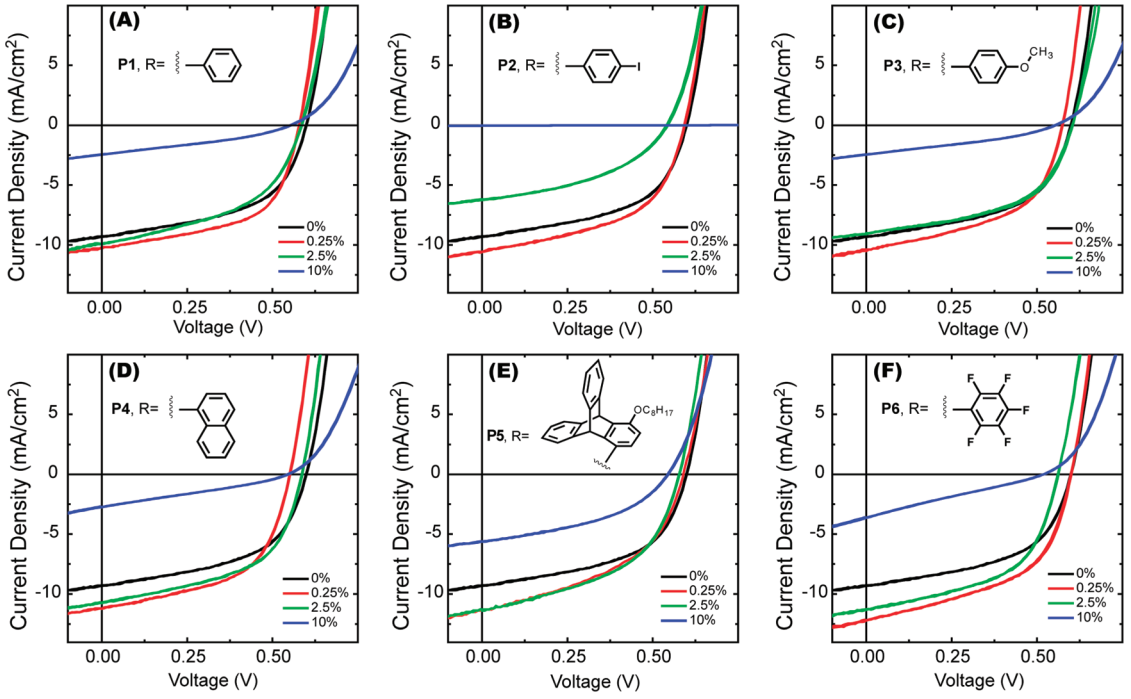

Figure 3. *J*−*V* curves under 1 sun for solar cells containing 50/50 total polymer/$PC_{61}BM$ with varying amounts (0% black, 0.25% red, 2.5% green, 10% blue) of P1−6. The average *J*−*V* curves from eight different devices are shown in each case. Panels A−F correspond to additives P1−6, respectively. The insets show the structure of the functional group attached to the side chain of the corresponding additive.

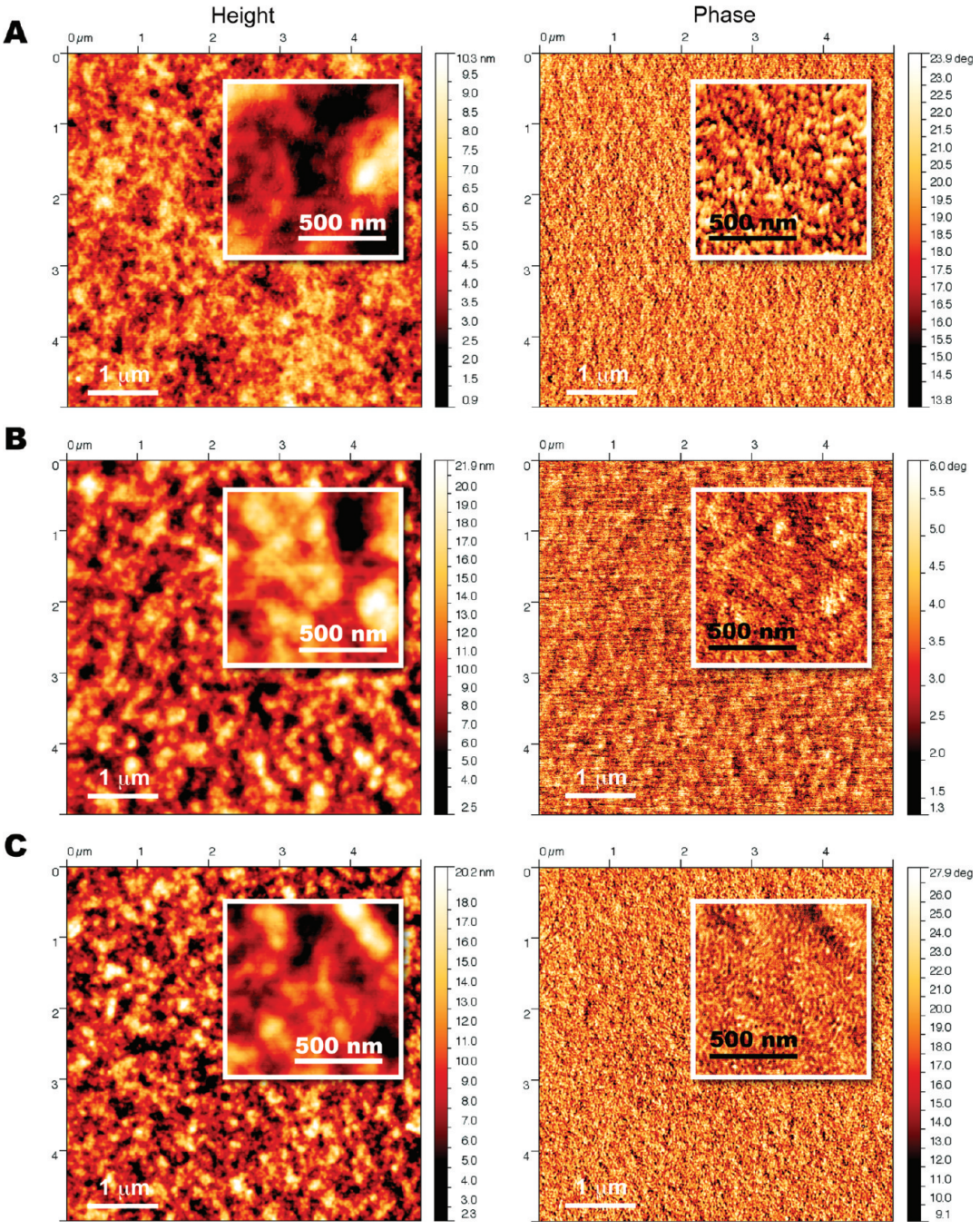

Figure 4. Tapping-mode atomic force microscopy images of a 5 μm $\times$ 5 μm region of three films used in making devices shown in Figures 1 and 3. (A) 1:1 P3HT/$PC_{61}BM$. (B) 1:1 (P3HT + 0.25 wt % P6) to $PC_{61}BM$. (C) 1:1 (P3HT + 2.5 wt % P6) to $PC_{61}BM$. (A–C) Topography of each film is shown in the left panels and the corresponding phase images in the right panels. Insets show the topography and corresponding phase images for a smaller scan area (1 μm $\times$ 1 μm) of the same films.

regions of each film are as follows: 1.51 $\pm$ 0.02 for 0 wt % **P6**; 3.00 $\pm$ 0.01 for 0.25 wt % **P6**; and 2.98 $\pm$ 0.02 for 2.5 wt % **P6**. With **P6** loadings as small as 0.25 wt %, the average surface roughness is double that of P3HT/$PC_{61}BM$ films, therefore suggesting that aromatic moieties present at side-chain termini are capable of significantly affecting the morphology of polymer–fullerene blends. Very different morphologies are indeed observed for the three different blends in their phase images (Figure 4, right panels). Bicontinuous networks of nanoscale fibrillar features are apparent in Figure 4A,B for films containing 0 and 0.25 wt % **P6**, respectively. However, the phase images of films containing 2.5 wt % **P6** reveal the presence of isolated clusters with relatively large domain widths (up to 30 nm). These observations are consistent with the loading-dependent *J*–*V* curves shown in Figure 3, wherein higher **P6** loadings lead to decreased V_{OC} and J_{SC} values and increased series resistances.

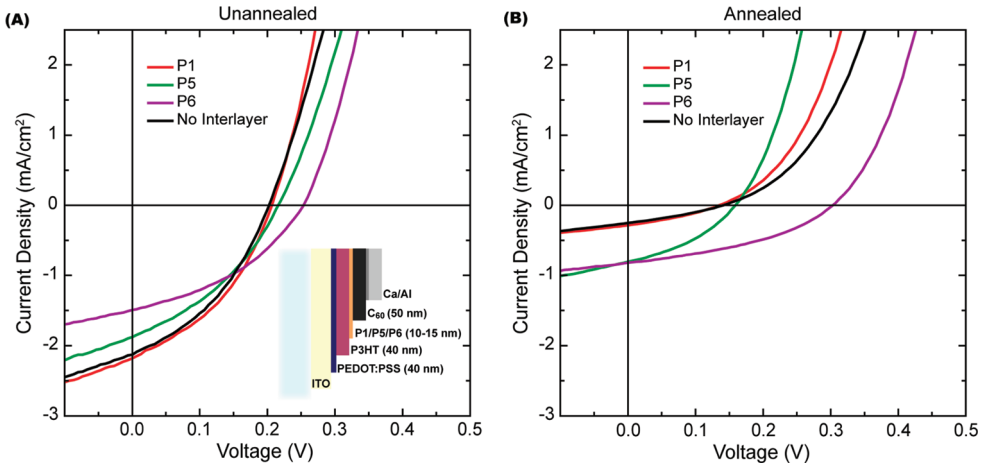

Figure 5. Devices containing discrete layers of P3HT, side-chain-functionalized poly(thiophene)s, and C_{60}. (A) $J-V$ curves under illumination of as-deposited, planar devices. The inset depicts the layered device architecture, with the thickness of each layer provided. (B) $J-V$ curves under illumination of the same devices as in (A) after annealing at 150 °C under nitrogen for 1 h to create a planar-mixed heterojunction. A reference P3HT/C_{60} device lacking a layer of the side-chain-functionalized additive is shown in black.

In order to further characterize the effects of the side-chain-functionalized additives on device performance in the absence of morphological factors, we fabricate layered solar cells. Specifically, devices containing discrete layers of P3HT, fullerene, and a side-chain-functionalized poly(thiophene) are studied to ascertain whether the side-chain moiety can introduce a dipole at the polymer–fullerene interface and thus increase the observed V_{OC}.[38,39] Our device structure is as follows: ITO/PEDOT:PSS/P3HT/additive/C_{60}/Ca/Al (Figure 5). Discrete layers of P3HT and **P1**, **P5**, or **P6** are obtained by first spin-casting a layer of P3HT from 1,2-dichlorobenzene and annealing it at 150 °C, then spin-casting a layer of the appropriate additive from dichloromethane (DCM) solutions. The procedure of using DCM as an orthogonal solvent for high molecular rr-P3HT has been previously reported.[40] The high molecular weight rr-P3HT used in this study is insoluble in DCM; however, polymer additives **P1**–**6** are solubilized by DCM, thus allowing for their deposition onto rr-P3HT with minimal layer mixing. A 50 nm thick layer of C_{60}, followed by layers of calcium (25 nm) and aluminum (80 nm), is then deposited by thermal evaporation under high vacuum.

Appropriate metrics for the devices examined in Figure 5 are tabulated in the Supporting Information (Table S3). Indeed, when a thin layer (15 ± 5 nm) of **P1**, **P5**, or **P6** is introduced between layers of P3HT (40 nm) and C_{60} (50 nm), a 3, 13, and 51 mV increase, respectively, in the V_{OC} of the solar cell is observed compared to P3HT/C_{60} devices lacking an interlayer (Figure 5). Furthermore, this increase in V_{OC} is preserved upon thermally annealing the layered device, which encourages the formation of a planar-mixed heterojunction.[41,42] In the case of the planar-mixed heterojunctions thus formed, higher J_{SC} and FF values, in addition to increased V_{OC} values, are observed in the presence of **P5** and **P6**, similar to previous observations in ternary P3HT/PC_{61}BM devices.

The calculated dipole moments (B3LYP-6-31G*) of the six *isolated* side-chain moieties found in **P1**–**6** are provided in the Supporting Information (Figure S5). Additionally, the calculated dipole moments of the six side-chain-functionalized *thiophene repeat units* found in **P1**–**6** are provided in Figure S6. The dipole moments of the side-chain-functionalized repeat units contained in **P1**, **P5**, and **P6** are calculated to be 0.52, 1.58, and 2.43 D, respectively. Therefore, the trend in the strength of the dipole moments within this family of additives qualitatively concurs with the trend in the V_{OC} increase observed with additive interlayers. Additive **P6** contains pentafluorophenyl ether side-chain moieties that display the largest isolated dipole moments and, correspondingly, leads to the largest observed increase in V_{OC} in layered devices.

Additive Regioregularity. Varying the regioregularity and the degree of substitution of the best-performing additive **P6** significantly diminishes its ability to yield higher J_{SC} values. Analogues of **P6** with varying degress of disorder are synthesized (see Supporting Information for synthetic details) and studied as additives to the P3HT/PC_{61}BM BHJ: a random but regioregular copolymer, **P6a**; a regioregular homopolymer **P6b**; and a random, regiorandom copolymer **P6c** (Figure 6A). The ^{1}H NMR signals of additives **P6** and **P6a**–**c** in the diagnostic aromatic region are shown in Figure 6B; as expected, increasing disorder in the polymer backbone leads to broadening of the aromatic signal at 6.8 ppm. PVs containing the random, regioregular copolymer **P6a** display lower J_{SC} values compared to those containing the AB-alternating regioregular polymer **P6** (averaged over eight devices, Figure 6C). In the case of a regiorandom random copolymer, **P6c**, little effect on J_{SC} values is observed

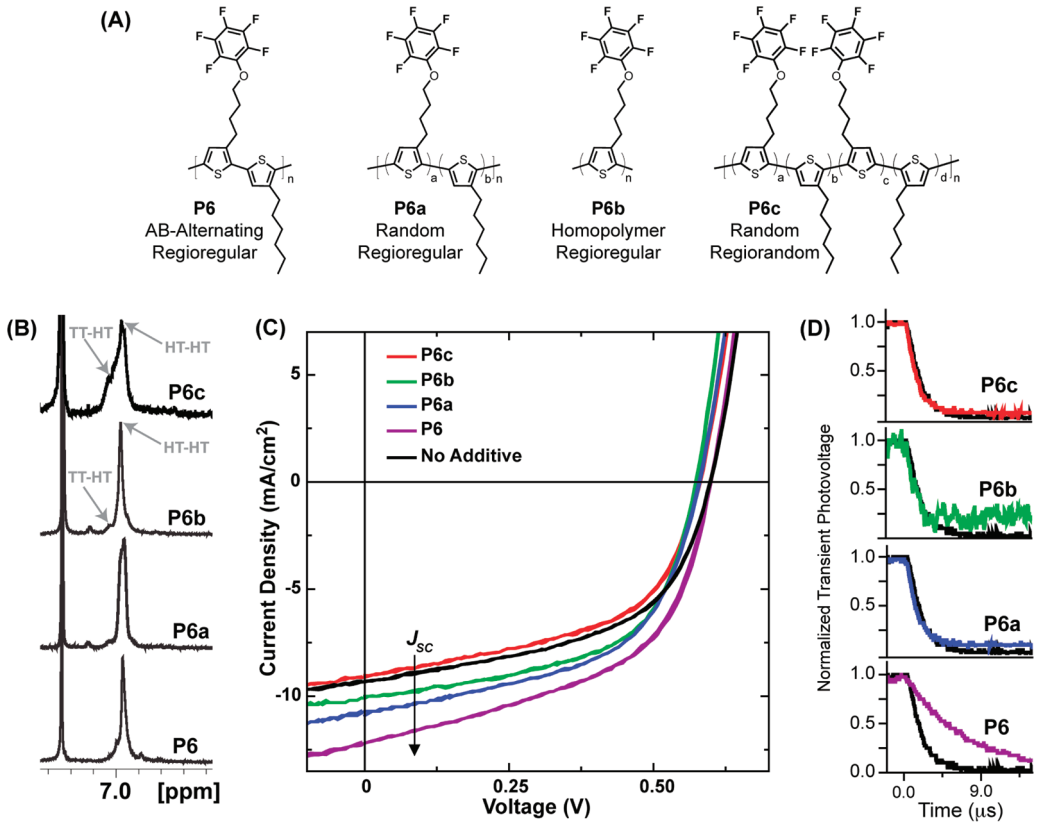

Figure 6. Study of the influence of additive copolymer composition and regioregularity. (A) Structures of P6 and its analogues with varying degrees of disorder. (B) ^{1}H NMR signals of P6 and P6a−c in the aromatic region showing very sharp signals for the H in the 4-position of the polymer backbone for regioregular polymers (P6, P6a, P6b). Regiorandom P6c shows an additional shoulder. (C) $J-V$ curves under 1 sun for solar cells containing a 1:1 ratio of total polymer (P3HT + 0.25 wt % P6a−c) to $PC_{61}BM$ and for a reference device with no additive (black). Average $J-V$ curves for eight different devices are shown. (D) Normalized transient photovoltage decay curves at V_{OC} for the same devices as in (C). Bias illumination was 100 mW/cm^2 white light giving V_{OC} values of 0.59 V for P3HT/$PC_{61}BM$, 0.60 V for additive P6, 0.58 for additives P6a and P6c, and 0.57 V for additive P6b. The secondary pulse was from a 635 nm laser, length 5 s.

with ternary mixtures relative to a P3HT/$PC_{61}BM$ control. The effects of homopolymer **P6b** fall between those of **P6a** and **P6c**. Small-perturbation transient open circuit voltage decay measurements of charge carrier lifetime in the presence of these disordered additives reveal that only the AB-alternating regioregular polymer **P6** results in increased charge carrier lifetimes compared to a reference cell (Figure 6D).

Fullerene Loading. The J_{SC} values for solar cells containing 0.25 wt % **P6** with varying ratios of polymer to either $PC_{61}BM$ or $PC_{71}BM$ are shown in Figure 7 (see the Supporting Information for other device metrics). Notable increases in J_{SC} in the presence of **P6** are only obtained for polymer/fullerene ratios of 1:1 for both $PC_{61}BM$ and $PC_{71}BM$. Previous studies have shown that for high molecular weight, regioregular P3HT, a polymer fullerene ratio of 1:1 leads to optimal PCEs,[43,44] consistent with the data presented in Figure 7.

Active Layer Thickness. In order to investigate the effects of the best-performing additive, **P6**, on solar cells containing a thicker active layer, devices containing a 220 nm thick bulk heterojunction are fabricated (see Figure S5 in the Supporting Information). It has been demonstrated that P3HT/PCBM bulk heterojunction solar cells should be approximately 220 nm thick to achieve an optimal PCE of 4.5−5%.[2] Using an active layer compostion of 49.75 wt % P3HT, 0.25 wt % **P6**, and 50 wt % $PC_{61}BM$ (which yields the maximal PCE increase in 75 nm thick devices according to the aforementioned experiments), a PCE of up to 5.3% is achieved with 220 nm thick solar cells (30% PCE increase over a control device lacking **P6**; see Supporting Information).

DISCUSSION

A proposed model of the nanoscale organization within ternary blends of **P1**−**6**, rr-P3HT, and PC_nBM is depicted in Figure 8B. On the basis of the combined observations that additives **P1**−**6** do not disrupt the crystallinity of the P3HT phase in ternary blends and that only AB-alternating regioregular analogues improve the performance of OPV devices, we propose that the side-chain-functionalized additives selectively localize at the rr-P3HT−fullerene interface, likely in the amorphous region of P3HT where the P3HT domains contain approximately 20% (in volume) of PCBM.

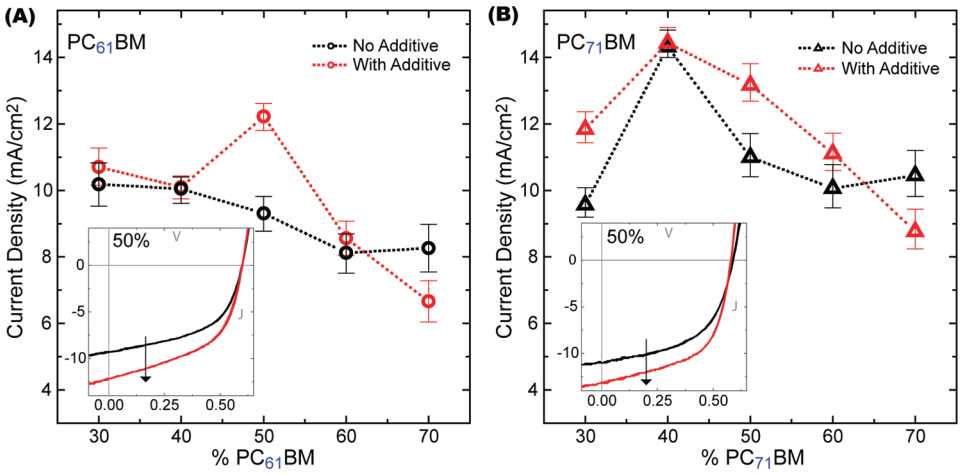

Figure 7. Study of the influence of fullerene structure and loading. J_{SC} for solar cells containing 0.25 wt % of pentafluorophenol additive P6 with varying ratios of total polymer/PC_nBM compared to reference devices for $PC_{61}BM$ (A, circles) and $PC_{71}BM$ (B, triangles). J_{SC} values for solar cells of the same composition with no additive are shown in black. The inset shows the $J-V$ curves under 1 sun for solar cells containing 50/50 total polymer/PC_nBM with (red) and without (black) P6. Average J_{SC} values from eight different devices are reported.

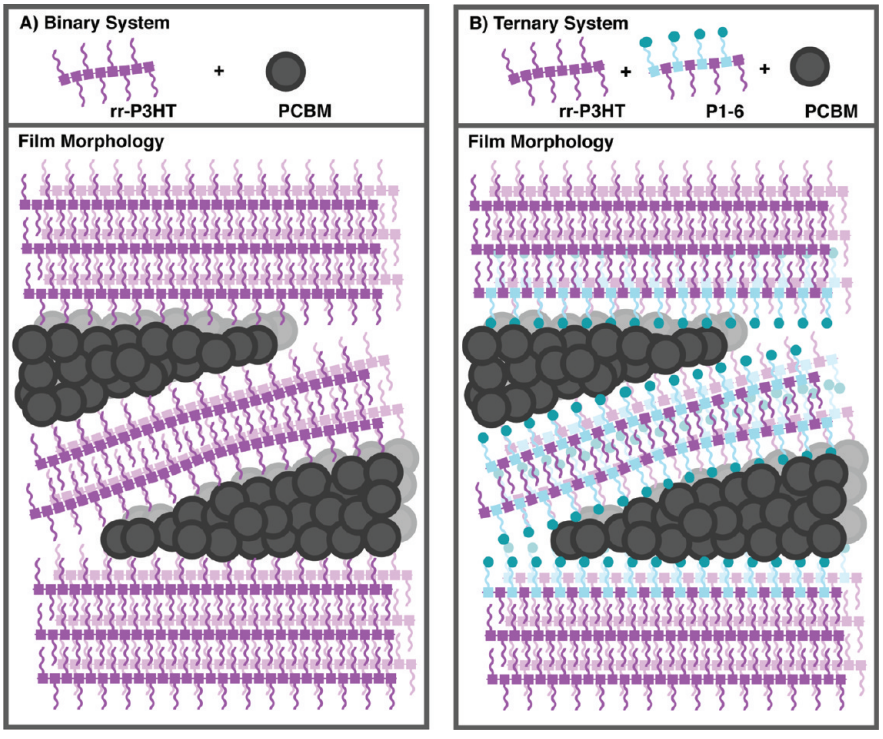

Figure 8. Diagram of the proposed nanoscale organization within (A) binary mixtures of rr-P3HT and PC_nBM and (B) ternary mixtures of rr-P3HT, PC_nBM, and side-chain-functionalized poly(thiophene)s P1−6. Additives P1−6 are proposed to selectively localize at the polymer−fullerene heterointerface, and the aromatic moieties at side-chain termini are proposed to interact with the fullerene phase. Depending on the exact structure of the side-chain functional group, a dipole is introduced across the polymer−fullerene heterointerface that decreases charge carrier recombination.

In recent years, several studies have revealed the importance of these regions and the effect they have in solar cell performance since they highly influence the optoelectronic properties of the resulting heterojunction.[45,46] For this reason, the presence of additives in this region should have a large effect in solar cell performance.

Given the marked difference in steady-state quenching responses and solar cell performance metrics between polymers **P1**−**6**, we infer that aromatic moieties present at side-chain termini interact with fullerenes and that the exact nature and identity of the side-chain aromatic moieties influences the degree of this interaction. Since the presence of a side-chain-functionalized

poly(thiophene) layer leads to increased V_{OC} values in layered devices, we conclude that aromatic moieties at side-chain termini are capable of inducing a dipole at the polymer–fullerene interface. Moreover, we believe that this induced dipole is responsible for the increased charge carrier lifetimes and higher photocurrents observed in bulk heterojunctions containing side-chain-functionalized poly(thiophene)s. On the basis of the results presented herein, we suggest that side-chain functionalization is an as-of-yet underexplored strategy to design polymeric additives that improve the power conversion efficiencies of polymer solar cells by fine-tuning charge transfer phenomena at the polymer–fullerene interface.

CONCLUSIONS

The motivation of this study is to determine if small amounts of designer additives placed at the polymer–fullerene interface in bulk heterojunction (BHJ) solar cells can influence their performance. A series of AB-alternating side-chain-functionalized poly(thiophene) additives, **P1**–**6**, are designed to selectively localize at the interface between regioregular poly(3-hexylthiophene) (rr-P3HT) and PC_nBM (n = 61, 71) phases and are synthesized using GRIM polymerization methods from corresponding bithiophene monomers. Phenoxy (**P1**), 4-iodophenoxy (**P2**), 4-anisyloxy (**P3**), 1-naphthoxy (**P4**), triptycene (**P5**), and perfluorophenoxy (**P6**) groups are introduced at alternating side-chain termini along a regioregular poly(thiophene) backbone. The side-chain-functionalized poly(thiophene)s **P1**–**6** display the same photophysical properties as commercial regioregular poly(3-hexylthiophene) (rr-P3HT). Although neat films of **P1**–**6** are found to be amorphous, the presence of up to 10 wt % **P1**–**6** in rr-P3HT/$PC_{61}BM$ blends does not disrupt the advantageous formation of P3HT lamellae within this ternary mixture.

BHJ solar cells containing ternary mixtures of rr-P3HT, PC_nBM (n = 61, 71), and varying weight ratios of additives **P1**–**6** are fabricated and characterized. At low loadings (0.25 wt %), the presence of **P1**–**6** consistently increases the short circuit current (J_{SC}) and decreases the series resistance (R_s) of the corresponding photovoltaic cells, leading to an increase in the power conversion efficiency (PCE) compared to reference P3HT/$PC_{61}BM$ cells. Small-perturbation transient open circuit voltage decay measurements reveal that, at 0.25 wt % incorporation, additives **P1**–**6** increase charge carrier lifetimes in P3HT/$PC_{61}BM$ solar cells. Higher additive loadings (>5 wt %) lead to detrimental nanoscale phase separation within the active layer blend and produce solar cells with high series resistances and low overall PCEs. Perfluorophenoxy-containing polymer **P6** is the most effective side-chain-functionalized additive and yields a 28% increase in PCE when incorporated into the rr-P3HT/$PC_{61}BM$ BHJ at a 0.25 wt % loading. Moreover, the regioregularity and copolymer composition of the side-chain-functionalized poly(thiophene)s is found to significantly affect their efficacy as additives in solar cells, with only the regioregular AB-alternating copolymer **P6** yielding a large increase in PCE. Devices with 220 nm thick BHJs containing 0.25 wt % **P6** are fabricated and display PCE values of up to 5.3% (30% PCE increase over a control device lacking **P6**).

We propose that the regioregular additives **P1**–**6** selectively localize at the interface between rr-P3HT and PC_nBM such that the functional groups at side-chain termini interact with the fullerene phase. We believe that these side-chain aromatic moieties introduce a dipole at the polymer–fullerene interface, which decreases the rate of bimolecular recombination and, therefore, improves charge collection across the active layer in a bulk heterojunction polymer solar cell.

EXPERIMENTAL METHODS

General Procedure for Monomer (M) Synthesis. Compound **1** was synthesized following modified literature procedures (see Supporting Information). To a solution of an appropriate phenol (1.5 equiv) in EtOH was added KOH (1.7 equiv), and the mixture was stirred for 10 min. Compound **1** and a spatula tip-full of NaI was added and the reaction subsequently refluxed under argon for 2 h. After addition of H_2O, the reaction was extracted with ether (3×, 50 mL), and the combined organic phases were washed with water (2×, 50 mL) and brine and dried over magnesium sulfate. After solvent removal, the resulting oil was purified by column chromatography.

General Procedure for Polymer Additive (P) Synthesis. To a solution of the appropriate monomer **M** (1 equiv) in dry THF was added ^{t}BuMgCl (1.0 M in THF, 1 equiv) at room temperature, and the reaction was subsequently heated to 70 °C. After stirring for 2 h, Ni(dppp)Cl_2 (1.4 mol %) dispersed in 1 mL of dry THF was added *via* cannula. The reaction was observed to immediately turn deep orange and fluorescent yellow. After stirring for 10 h, excess methanol was added to the reaction mixture to precipitate the polymer. The resulting dark purple solid was reprecipitated twice with $CHCl_3$/MeOH, subjected to Soxhlet extraction with MeOH and acetone, and subsequently extracted with $CHCl_3$ to isolate the desired polymer sample.

Device Fabrication. Prepatterned indium tin oxide (ITO)-coated glass substrates (Thin Film Devices, Inc.) were sonicated in acetone (30 min) and isopropyl alcohol (30 min) and oxygen plasma-cleaned (3 min) immediately prior to deposition of the PEDOT:PSS layer. PEDOT:PSS (2–5 wt % in water, Aldrich) was spin-coated in a nitrogen atmosphere at 4000 rpm and annealed at 150 °C (using a hot plate) for 15 min under nitrogen. A 40 nm PEDOT layer was thus obtained. Film thickness was determined by ellipsometry measurements on separate films prepared on silicon substrates. For the active layer, a 10 mg/mL solution of 1:1 total polymer/PC_nBM in 1,2-dichlorobenzene

(DCB) was employed (in a representative example, 1.9 mg of P3HT, 0.1 mg of **P1**, and 2 mg of $PC_{61}BM$ were dissolved in 0.2 mL of DCB). Then, 60 μL of this solution was spin-coated onto the PEDOT layer at 1000 rpm under nitrogen. The substrate was taken from the spin chuck and immediately placed under an inverted Petri dish inside the glovebox for 10 min to encourage solvent annealing from the small amount of residual DCB on the substrate. Next, the solar cells were placed on a 150 °C hot plate and annealed for 45 min under nitrogen. A 75 $\pm$ 5 nm active layer was thus obtained. A 220 nm thick active layer was obtained following the same procedure, with the exception of using a 30 mg/mL solution of 1:1 total polymer/PC_nBM in DCB. Following this deposition procedure, the top electrode was deposited by thermal evaporation of a 25 nm thick film of Ca followed by an 80 nm thick film of Al. The device area, as defined by the anode–cathode overlap, is 1.21 mm^2.

Device Characterization. Current density–voltage (*J*–*V*) measurements were recorded by a Keithley 6487 picoammeter both in the dark and under illumination. The devices were illuminated through the glass substrate using an Oriel 91191 150 W full spectrum solar simulator. The illumination intensity was calibrated to 100 mW/cm^2 using an NREL-certified silicon photodiode. Spectral mismatch was not corrected for these measurements. For measurement of external quantum efficiencies, the sample was illuminated with optically chopped broadband light from a 1000 W Xe lamp focused into an Acton Spectrapro 300i monochromator that underfilled the device area. A calibrated silicon photodetector was used to measure the optical power of the output, which was subsequently focused onto the device under study. A SRS-830 lock-in amplifier provided with the reference signal from the optical chopper (45 Hz) was used to extract a measurement of the AC photocurrent. For the small-perturbation transient photovoltage measurement, a Newport LQD laser diode (λ 635 nm) driven by an Agilent 33220A function generator (11 Hz, 50% duty cycle) was used as a second light source to provide square wave modulated illumination. This illumination was filtered through a neutral density filter before reaching the device to ensure a small (<5%) illumination perturbation. V_{OC} decay transients were recorded on a Tektronix TDS 3054B digital oscilloscope with a Tektronix ADA440A high impedance differential preamplifier.

Conflict of Interest: The authors declare no competing financial interest.

Acknowledgment. This work was supported by Eni SpA under the Eni-MIT Solar Frontiers Center.

Supporting Information Available: XRD data, external quantum efficiencies, tabulated metrics for all devices reported, dipole moment calculations, and synthetic procedures and spectroscopic characterization data for **M1**–**6** and **P1**–**6**. This material is available free of charge *via* the Internet at http://pubs.acs.org.

REFERENCES AND NOTES

1. Barr, M. C.; Rowehl, J. A.; Lunt, R. R.; Xu, J.; Wang, A.; Boyce, C. M.; Im, S. G.; Bulović, V.; Gleason, K. K. Direct Monolithic Integration of Organic Photovoltaic Circuits on Unmodified Paper. *Adv. Mater.* **2011**, *23*, 3500–3505.
2. Coakley, K. M.; McGehee, M. D. Conjugated Polymer Photovoltaic Cells. *Chem. Mater.* **2004**, *16*, 4533–4542.
3. Brabec, C. J.; Gowrisanker, S.; Halls, J. J. M.; Laird, D.; Jia, S.; Williams, S. P. Polymer–Fullerene Bulk-Heterojunction Solar Cells. *Adv. Mater.* **2010**, *22*, 3839–3856and references therein.
4. Forrest, S. R. The Limits to Organic Photovoltaic Cell Efficiency. *MRS Bull.* **2005**, *30*, 28–32.
5. Wu, F.-C.; Huang, Y.-C.; Cheng, H.-L.; Chou, W.-Y.; Tang, F.-C. Importance of Disordered Polymer Segments to Microstructure-Dependent Photovoltaic Properties of Polymer–Fullerene Bulk Heterojunction Solar Cells. *J. Phys. Chem. C* **2011**, *115*, 15057–15066.
6. Yin, W.; Dadmun, M. A New Model for the Morphology of P3HT/PCBM Organic Photovoltaics from Small-Angle Neutron Scattering: Rivers and Streams. *ACS Nano* **2011**, *5*, 4756–4768.
7. Hopkinson, P. E.; Staniec, P. A.; Pearson, A. J.; Dunbar, A. D. F.; Wang, T.; Ryan, A. J.; Jones, R. A. L.; Lidzey, D. G.; Donald, A. M. A Phase Diagram of the P3HT:PCBM Organic Photovoltaic System: Implications for Device Processing and Performance. *Macromolecules* **2011**, *44*, 2908–2917.
8. Kozub, D. R.; Vakhshouri, K.; Orme, L. M.; Wang, C.; Hexemer, A.; Gomez, E. D. Polymer Crystallization of Partially Miscible Polythiophene/Fullerene Mixtures Controls Morphology. *Macromolecules* **2011**, *44*, 5722–5726.
9. Kiel, J. W.; Mackay, M. E.; Kirby, B. J.; Maranville, B. B.; Majkrzak, C. F. Phase-Sensitive Neutron Reflectometry Measurements Applied in the Study of Photovoltaic Films. *J. Chem. Phys.* **2010**, *133*, 074902.
10. Lee, J. K.; Ma, W. L.; Brabec, C. J.; Yuen, J.; Moon, J. S.; Kim, J. Y.; Lee, K.; Bazan, G. C.; Heeger, A. J. Processing Additives for Improved Efficiency from Bulk Heterojunction Solar Cells. *J. Am. Chem. Soc.* **2008**, *130*, 3619–3623.
11. Tsai, J.-H.; Lai, Y.-C; Higashihara, T.; Lin, C.-J.; Ueda, M.; Chen, W.-C. Enhancement of P3HT/PCBM Photovoltaic Efficiency Using the Surfactant of Triblock Copolymer Containing Poly(3-hexylthiophene) and Poly(4-vinyltriphenylamine) Segments. *Macromolecules* **2010**, *43*, 6085–6091.
12. Sivula, K.; Ball, Z. T.; Watanabe, N.; Fréchet, J. M. J. Amphiphilic Diblock Copolymer Compatibilizers and Their Effect on the Morphology and Performance of Polythiophene: Fullerene Solar Cells. *Adv. Mater.* **2006**, *18*, 206–210.
13. Yang, C.; Lee, J. K.; Heeger, A. J.; Wudl, F. Well-Defined Donor–Acceptor Rod–Coil Diblock Copolymers Based on P3HT Containing C60: The Morphology and Role as a Surfactant in Bulk-Heterojunction Solar Cells. *J. Mater. Chem.* **2009**, *19*, 5416–5423.
14. Campoy-Quiles, M.; Kanai, Y.; El-Basaty, A.; Sakai, H.; Murata, H. Ternary Mixing: A Simple Method To Tailor the Morphology of Organic Solar Cells. *Org. Electron.* **2009**, *10*, 1120–1132.
15. Nguyen, L. H.; Hoppe, H.; Erb, T.; Günes, S.; Gobsch, G.; Sariciftci, N. S. Effects of Annealing on the Nanomorphology and Performance of Poly(alkylthiophene):Fullerene Bulk-Heterojunction Solar Cells. *Adv. Funct. Mater.* **2007**, *17*, 1071–1078.
16. Wu, P.-T.; Ren, G.; Jenekhe, S. A. Crystalline Random Conjugated Copolymers with Multiple Side Chains: Tunable Intermolecular Interactions and Enhanced Charge Transport and Photovoltaic Properties. *Macromolecules* **2010**, *43*, 3306–3313.
17. Mondal, R.; Ko, S.; Verploegen, E.; Becerril, H. A.; Toney, M. F.; Bao, Z. Side Chain Engineering of Fused Aromatic Thienopyrazine Based Low Band-Gap Polymers for Enhanced Charge Carrier Mobility. *J. Mater. Chem.* **2011**, *21*, 1537–1543.
18. Thompson, B. C.; Kim, B. J.; Kavulak, D. F.; Sivula, K.; Mauldin, C.; Fréchet, J. M. J. Influence of Alkyl Substitution Pattern in Thiophene Copolymers on Composite Fullerene Solar Cell Performance. *Macromolecules* **2007**, *40*, 7425–7428.
19. Moulé, A. J.; Allard, S.; Kronenberg, N. M.; Tsami, A.; Scherf, U.; Meerholz, K. The Effect of Polymer Nanoparticle Formation on the Efficiency of Polythiophene-Based Bulk Heterojunctions. *J. Phys. Chem. C* **2008**, *112*, 12583–12589.
20. Mayer, A. C.; Toney, M. F.; Scully, S. R.; Rivnay, J.; Brabec, C. J.; Scharber, M.; Koppe, M.; Heeney, M.; McCulloch, I.; McGehee, M. D. Bimolecular Crystals of Fullerenes in Conjugated Polymers and the Implications of Molecular Mixing for Solar Cells. *Adv. Funct. Mater.* **2009**, *19*, 1173–1179.
21. Ohshimizu, K.; Takahashi, A.; Rho, Y.; Higa-shihara, T.; Ree, M.; Ueda, M. Synthesis and Characterization of Polythiophenes Bearing Aromatic Groups at the 3-Position. *Macromolecules* **2011**, *44*, 719–727.
22. Stokes, K. K.; Heuzé, K.; McCullough, R. D. New Phosphonic Acid Functionalized, Regioregular Polythiophenes. *Macromolecules* **2003**, *36*, 7114–7118.

23. Bjørnholm, T.; Greve, D. R.; Reitzel, N.; Has-senkam, T.; Kjaer, K.; Howes, P. B.; Larsen, N. B.; Bøgelund, J.; Jayaraman, M.; Ewbank, P. C.; *et al.* Self-Assembly of Regioregular, Amphiphilic Polythiophenes into Highly Ordered π-Stacked Conjugated Polymer Thin Films and Nanocircuits. *J. Am. Chem. Soc.* **1998**, *120*, 7643–7644.
24. Wang, F.; Yang, Y.; Swager, T. M. Carbon Nanotube/Polythiophene Chemiresistive Sensors for Chemical Warfare Agents. *Angew. Chem., Int. Ed.* **2008**, *47*, 8394–8396.
25. Veen, E. M.; Postma, P. M.; Jonkman, H. T.; Spek, A. L.; Feringa, B. L. Solid State Organisation of C60 by Inclusion Crystallisation with Triptycenes. *Chem. Commun.* **1999**, 1709–1710.
26. McCullough, R. D.; Lowe, R. D. Enhanced Electrical Conductivity in Regioselectively Synthesized Poly(3-alkylthiophenes). *Chem. Commun.* **1992**, 70–72.
27. Loewe, R. S.; Khersonsky, S. M.; McCullough, R. D. A Simple Method To Prepare Head-to-Tail Coupled, Regioregular Poly(3-alkylthiophenes) Using Grignard Metathesis. *Adv. Mater.* **1999**, *11*, 250–253.
28. Loewe, R. S.; Ewbank, P. C.; Liu, J.; Zhai, L.; McCullough, R. D. Regioregular, Head-to-Tail Coupled Poly(3-alkylthiophenes) Made Easy by the GRIM Method: Investigation of the Reaction and the Origin of Regioselectivity. *Macromolecules* **2001**, *34*, 4324–4333.
29. For examples of GRIM polymerizations used to obtain alternating AB copolymers from the corresponding 5,5′-dibromo-2,2′-bithiophene monomer, see: Wang, B.; Watt, S.; Hong, M.; Domercq, B.; Sun, R.; Kippelen, B.; Collard, D. M. Synthesis, Properties, and Tunable Supramolecular Architecture of Regioregular Poly(3-alkylthiophene)s with Alternating Alkyl and Semifluoroalkyl Substituents. *Macromolecules* **2008**, *41*, 5156–5165.
30. Benanti, T. L.; Kalaydjian, A.; Venkataraman, D. Protocols for Efficient Postpolymerization Functionalization of Regioregular Polythiophenes. *Macromolecules* **2008**, *41*, 8312–8315.
31. Hong, X. M.; Tyson, J. C.; Collard, D. M. Controlling the Macromolecular Architecture of Poly(3-alkylthiophene)s by Alternating Alkyl and Fluoroalkyl Substituents. *Macromolecules* **2000**, *33*, 3502–3504.
32. Kim, Y.; Cook, S.; Tuladhar, S. M.; Choulis, S. A.; Nelson, J.; Durrant, J. R.; Bradley, D. D. C.; Giles, M.; McCulloch, I.; Ha, C.-S.; *et al.* Strong Regioregularity Effect in Self-Organizing Conjugated Polymer Films and High-Efficiency Polythiophene:Fullerene Solar Cells. *Nat. Mater.* **2006**, *5*, 197–203.
33. Lenes, M.; Morana, M.; Brabec, C. J.; Blom, P. W. M. Recombination-Limited Photocurrents in Low Bandgap Polymer/Fullerene Solar Cells. *Adv. Funct. Mater.* **2009**, *19*, 1106–1111.
34. Mihailetchi, V. D.; Koster, L. J. A.; Blom, P. W. M.; Melzer, C.; de Boer, B.; van Duren, J. K. J.; Janssen, R. A. J. Compositional Dependence of the Performance of Poly(*p*-phenylene vinylene):Methanofullerene Bulk-Heterojunction Solar Cells. *Adv. Funct. Mater.* **2005**, *15*, 795–801.
35. O'Regan, B. C.; Scully, S.; Mayer, A. C.; Palomares, E.; Durrant, J. R. The Effect of Al_2O_3 Barrier Layers in TiO_2/Dye/CuSCN Photovoltaic Cells Explored by Recombination and DOS Characterization Using Transient Photovoltage Measurements. *J. Phys. Chem. B* **2005**, *109*, 4616–4623.
36. Zhao, N.; Osedach, T. P.; Chang, L.-Y.; Geyer, S. M.; Wanger, D.; Binda, M. T.; Arango, A. C.; Bawendi, M. G.; Bulović, V. Colloidal PbS Quantum Dot Solar Cells with High Fill Factor. *ACS Nano* **2010**, *4*, 3743–3752.
37. For an example of using topography and phase AFM images to study the nanoscale morphology of polymer/fullerene blends, see: Verploegen, E.; Mondal, R.; Bettinger, C. J.; Sok, S.; Toney, M. F.; Bao, Z. Effects of Thermal Annealing upon the Morphology of Polymer–Fullerene Blends. *Adv. Funct. Mater.* **2010**, *20*, 3519–3529.
38. For an example of the effects of interface modification on photovoltaic performance, see: Goh, C.; Scully, S. R.; McGehee, M. D. Effects of Molecular Interface Modification in Hybrid Organic–Inorganic Photovoltaic Cells. *J. Appl. Phys.* **2007**, *101*, 114503.
39. For a second example of the effects of interface modification on photovoltaic performance, see: Tada, A.; Geng, Y.; Wei, Q.; Hashimoto, K.; Tajima, K. Tailoring Organic Heterojunction Interfaces in Bilayer Polymer Photovoltaic Devices. *Nat. Mater.* **2011**, *10*, 450–455.
40. Ayzner, A. L.; Tassone, C. J.; Tolbert, S. H.; Schwartz, B. J. Reappraising the Need for Bulk Heterojunctions in Polymer–Fullerene Photovoltaics: The Role of Carrier Transport in All-Solution-Processed P3HT/PCBM Bilayer Solar Cells. *J. Phys. Chem. C* **2009**, *113*, 20050–20055.
41. For an example of forming a planar-mixed heterojunction between P3HT and $PC_{61}BM$ by thermally annealing a bilayer, see: Treat, N. D.; Brady, M. A.; Smith, G.; Toney, M. F.; Kramer, E. J.; Hawker, C. J.; Chabinyc, M. L. Interdiffusion of PCBM and P3HT Reveals Miscibility in a Photovoltaically Active Blend. *Adv. Energy Mater.* **2011**, *1*, 82–85.
42. For a second example of forming a planar-mixed heterojunction between P3HT and $PC_{61}BM$ by thermally annealing a bilayer, see: Gevaerts, V. S.; Koster, L. J. A.; Wienk, M. M.; Janssen, R. A. J. Discriminating between Bilayer and Bulk Heterojunction Polymer:Fullerene Solar Cells Using the External Quantum Efficiency. *ACS Appl. Mater. Interfaces* **2011**, *3*, 3252–3256.
43. Sanyal, M.; Schmidt-Hansberg, B.; Klein, M. F. G.; Munuera, C.; Vorobiev, A.; Colsman, A.; Scharfer, P.; Lemmer, U.; Schabel, W.; Dosch, H.; *et al.* Effect of Photovoltaic Polymer/Fullerene Blend Composition Ratio on Microstructure Evolution during Film Solidification Investigated in Real Time by X-ray Diffraction. *Macromolecules* **2011**, *44*, 3795–3800.
44. Nicolet, C.; Deribew, D.; Renaud, C.; Fleury, G.; Brochon, C.; Cloutet, E.; Vignau, L.; Wantz, G.; Cramail, H.; Geoghegan, M.; *et al.* Optimization of the Bulk Heterojunction Composition for Enhanced Photovoltaic Properties: Correlation between the Molecular Weight of the Semiconducting Polymer and Device Performance. *J. Phys. Chem. B* **2011**, *115*, 12717–12727.
45. Chen, D.; Liu, F.; Wang, C.; Nakahara, A.; Russell, T. P. Bulk Heterojunction Photovoltaic Active Layers *via* Bilayer Interdiffusion. *Nano Lett.* **2011**, *11*, 2071–2078.
46. Collins, B. A.; Tumbleston, J. R.; Ade, H. Miscibility, Crystallinity, and Phase Development in P3HT/PCBM Solar Cells: Toward an Enlightened Understanding of Device Morphology and Stability. *J. Phys. Chem. Lett.* **2011**, *2*, 3135–3145.